Veterinary Immunology and Immunopathology 271 (2024) 110741

Contents lists available at ScienceDirect

Veterinary Immunology and Immunopathology

journal homepage: www.elsevier.com/locate/vetimm

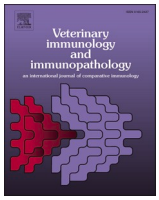

# Quantification of CD3, FoxP3, and granzyme B immunostaining in canine renal cell carcinoma

Ashleigh Cournoyer [a], Hayley Amerman [b], Charles-Antoine Assenmacher [b], Amy Durham [b], James A. Perry [a,1], Allison Gedney [a,2], Nicholas Keuler [c], Matthew J. Atherton [a,d], Jennifer A. Lenz [a,*]

[a] Department of Clinical Studies and Advanced Medicine, University of Pennsylvania, School of Veterinary Medicine, 3900 Spruce Street, Philadelphia, PA 19104, USA
[b] Department of Pathobiology, University of Pennsylvania, School of Veterinary Medicine, 3900 Spruce Street, Philadelphia, PA 19104, USA
[c] Department of Statistics, University of Wisconsin-Madison, 1300 University Ave, Madison, WI 53706, USA
[d] Department of Biomedical Sciences, University of Pennsylvania, School of Veterinary Medicine, 3900 Spruce Street, Philadelphia, PA 19104, USA

ARTICLE INFO

*Keywords:*
Tumor-infiltrating lymphocytes
T regulatory cells
Cytotoxic T lymphocytes
Dog
Gamma-glutamyl transferase

ABSTRACT

Tumor-infiltrating lymphocyte (TIL) density plays an important role in anti-tumor immunity and is associated with patient outcome in various human and canine malignancies. As a first assessment of the immune landscape of the tumor microenvironment in canine renal cell carcinoma (RCC), we retrospectively analyzed clinical data and quantified CD3, FoxP3, and granzyme B immunostaining in formalin-fixed paraffin-embedded tumor samples from 16 dogs diagnosed with renal cell carcinoma treated with ureteronephrectomy. Cell density was low for all markers evaluated. Increased numbers of intratumoral FoxP3 labelled (+) cells, as well as decreased granzyme B+: FoxP3+ TIL ratio, were associated with poor patient outcomes. Our initial study of canine RCC reveals that these tumors are immunologically cold and Tregs may play an important role in immune evasion.

## 1. Introduction

Renal cell carcinoma (RCC) follows a variable, yet often aggressive, clinical course in dogs with metastasis detected in 16–48% of patients at the time of diagnosis and 47–69% at the time of death (Bryan et al., 2006; Klein et al., 1987). Nephrectomy remains the treatment of choice for localized, unilateral tumors. Following nephrectomy, however, patient outcome can be difficult to predict and patients are at risk of tumor recurrence and metastasis, often occurring within the first year following surgery (Edmondson et al., 2015). Despite the known risk of metastasis, adjuvant chemotherapy has failed to improve patient outcome (Edmondson et al., 2015). Thus, there remains an unmet need to identify effective biomarkers and therapeutic targets in the treatment of canine RCC to reduce the risk of cancer progression and improve patient outcome.

Over the past decade, immune checkpoint inhibitors have revolutionized the treatment of metastatic RCC in humans resulting in durable responses (Gulati and Vaishampayan, 2020; Motzer et al., 2020). Multiple FDA-approved drugs targeting immune checkpoints, such as nivolumab and pembrolizumab, have been investigated and are being successfully incorporated into treatment regimens for human RCC (Powles et al., 2022; Sanchez-Gastaldo et al., 2017).The landscape of immunotherapeutics to treat canine cancer lag behind the advances for human RCC. Only recently has the FDA approved the first immune checkpoint inhibitor to treat canine cancer, Gilvetmab, a caninized monoclonal antibody targeting programmed cell death protein 1 (PD-1)(Merck Animal Health).

*Abbreviations:* TIL, tumor-infiltrating lymphocytes; CTL, cytotoxic T lymphocytes; Tregs, T regulatory cells; RCC, renal cell carcinoma; COX-2, cyclooxygenase-2; FFPE, formalin-fixed paraffin-embedded; IHC, immunohistochemistry; H&E, hematoxylin and eosin; PFS, progression free survival; OS, overall survival; GGT, gamma-glutamyl transferase; ALT, alanine transaminase; AST, aspartate transferase; ALP, alkaline phosphatase; MC, mitotic count; CT, computed tomography; CBC, complete blood count; MODS, multiple organ dysfunction syndrome; GZB, granzyme B; DAB, diaminobenzidine chromogen.

* Correspondence to: University of Pennsylvania, School of Veterinary Medicine, 3900 Spruce Street, Philadelphia, PA 19104, USA.
*E-mail address:* jlenz@upenn.edu (J.A. Lenz).
[1] Present address: Veterinary Referral Center of Central Oregon, 1820 NW Monterey Pines Drive, Bend, OR 97703, USA.
[2] Present address: Pet Emergency Treatment and Specialties, 930 North Queen Street, Lancaster, PA 17603, USA.

https://doi.org/10.1016/j.vetimm.2024.110741
Received 13 November 2023; Received in revised form 21 February 2024; Accepted 5 March 2024
Available online 16 March 2024

Currently, Gilvetmab is conditionally licensed by the USDA for the treatment of stage I, II, and III mast cell tumors and stage II and III melanoma. Several clinical trials to evaluate the safety and efficacy of Gilvetmab in dogs with cancer are ongoing, however, the utility of checkpoint inhibition in the treatment of canine RCC is unknown.

Coinciding with the recent approval of multiple immunotherapies in human oncology, tumor-

infiltrating lymphocytes (TIL) have garnered attention within the field of oncology, both for their prognostic significance and as a therapeutic strategy via adoptive cell therapy following isolation, *ex vivo* expansion, and reinfusion (Galon and Bruni, 2019; Kumar et al., 2021). Cytotoxic T lymphocytes represent a functionally important group of TIL due to their anti-tumor properties (Galon et al., 2006; Maibach et al., 2020). In contrast, infiltration of tumors with immunosuppressive regulatory T cells (Tregs) that generate immunosuppressive cytokines can lead to T cell dysfunction and immune evasion, resulting in poorer patient outcomes (Saleh and Elkord, 2020). Human RCC is generally considered an immunogenic tumor that frequently exhibits heavy TIL infiltrate, and several studies have documented that increased presence of immunosuppressive Tregs in human RCC correlates with a worse prognosis (Bai et al., 2021; Diaz-Montero et al., 2020; Griffiths et al., 2007; Jensen et al., 2009; Liotta et al., 2011; Senbabaoglu et al., 2016). Associations between TIL and patient outcome have also been found in various canine neoplasms, including mammary carcinoma, urothelial carcinoma, histiocytic sarcoma, and oral melanoma (Inoue et al., 2017; Kim et al., 2013; Lenz et al., 2022; Yasumaru et al., 2021). However, the presence of TIL and their potential associations with treatment outcome in canine RCC has not been investigated to date. To characterize TIL infiltrate, the current study evaluates CD3, a pan T-cell marker, as well as granzyme B (GZB), a key protease secreted by cytotoxic T lymphocytes to kill tumor cells, and FoxP3, the master transcriptional regulator of Tregs. Such information could help guide treatment, stratify patients as candidates for immunotherapy, and monitor treatment response.

Given the clinical significance of TIL identified in other urogenital tumors in dogs (Inoue et al., 2017;

Maeda et al., 2022), as well as in human RCC, the primary goal of our study was to evaluate CD3, FoxP3, and GZB positive immunostaining in canine RCC as an initial assessment of immunogenicity in this tumor type. A secondary aim of our study was to retrospectively analyze the association of these variables with patient outcome. We hypothesized that increased density of total TIL and GZB+ cells would be positively associated with survival, and increased FoxP3+ TIL density would be negatively associated with survival in dogs with

RCC.

## 2. Materials and methods

### 2.1. Study population

Medical records were retrospectively reviewed at the University of Pennsylvania Ryan Veterinary Hospital from 2008 to 2023 to identify dogs with a histologic diagnosis of RCC. Patients that underwent ureteronephrectomy with available tumor tissue for analysis were included. Clinical information collated from the medical record included: signalment (age, sex, neuter status, weight, breed), clinical signs at time of diagnosis, baseline hematology (complete blood count, serum chemistry), urinalysis, diagnostic imaging results, tumor size and lateralization, use of adjuvant chemotherapy, development of recurrence or metastasis, and survival time. Follow-up information not found within the medical record was obtained by contacting referring veterinarians and owners. All data in this study were obtained from materials collected during routine clinical care. Retrospective studies are exempt from review by the University of Pennsylvania Institutional Animal Care and Use Committee.

### 2.2. Histopathologic analyses

Hematoxylin and eosin (H&E) sections of stored tumor tissue were retrospectively evaluated by two

board-certified pathologists (HA, AD) to analyze: histologic subtype, clear cell morphology, mitotic count, Fuhrman nuclear grade, presence or absence of vascular invasion, degree of local invasiveness, and presence of sarcomatoid change. The neoplasms were assessed for clear cell cytologic features characterized by clear intracytoplasmic vacuoles and intricate vasculature and assigned histologic subtypes as solid, tubular, papillary, or cystic (multilocular cystic) based on the predominant morphology in the slides examined (Edmondson et al., 2015; Meuten, 2017). Solid carcinomas were characterized as having closely spaced neoplastic cells forming solid sheets or small lobules supported by minimal stroma. Tubular carcinomas were characterized by the neoplastic cells forming variably sized tubules separated by variable amounts of a fibrovascular stroma. Papillary carcinomas were characterized by neoplastic cells forming anastomosing cords and papilliferous fronds and projections lined by cuboidal epithelium supported by a fibrovascular stalk, often projecting into a lumen. Cystic/multilocular cystic carcinomas were characterized by a single or multiple large, central spaces devoid of tumor cells with cords, nests, or small papillary projections of neoplastic epithelial cells along the periphery of the cystic spaces. Sarcomatoid change was characterized by a transition of neoplastic epithelial cells from their histologic subtype into spindle-shaped cells arranged in interlacing streams and bundles that often demonstrate increased nuclear pleomorphism (Edmondson et al., 2015; Meuten, 2017).

The mitotic count was determined by counting 10 consecutive 400X high-power fields (2.37 $mm^2$)

within the areas of highest mitotic activity (Edmondson et al., 2015). The Fuhrman nuclear 4-tiered grading system was applied as previously described (Edmondson et al., 2015; Fuhrman et al., 1982), specifically evaluating and grading nuclear features based on nuclear diameter and shape, the prominence of nucleoli, and the presence of chromatin clumping. Vascular invasion was defined as the presence of neoplastic cells within the lumens of one or more vessels lined by vascular endothelium or evidence of neoplastic cells disrupting a vessel wall with extension of neoplastic cells into the lumen. Local invasion was defined as extension of neoplastic cells away from the main mass into the surrounding normal kidney parenchyma which may or may not have been accompanied by a desmoplastic response, and was categorized as none, mild, moderate, or severe.

### 2.3. Immunohistochemical analyses

Three separate 5 μm thick sections of formalin-fixed paraffin-embedded (FFPE) tumor sample were obtained for immunohistochemistry (IHC) and adhered to separate ProbeOn™ slides (Thermo Fisher Scientific). All tumor samples were then stained for CD3, FoxP3, and GZB as previously described (Lenz et al., 2022). Sections of canine tissues were stained as positive controls (Figure S1). Slides were subsequently scanned using the Aperio Versa 200 automatic slide scanner (Leica Biosystems) and visualized with the ImageScope software (Leica Biosystems). CD3 and FoxP3-positive cells were counted using cell counting algorithms available on Aperio ImageScope (Lenz et al., 2022). Automated cell counting via a digital image analysis algorithm could not be applied to GZB positive slides due to the distinctive pattern of granular stain uptake. Therefore, a manual count of GZB positive cells within ten randomly selected 1 $mm^2$ non-necrotic areas of the tumor was performed by a single investigator (JL) and normalized for tumors that had evidence of necrosis (i.e. if tumor appeared 10% necrotic at lower power magnification, the final count was multiplied by a factor of 0.9).

### 2.4. Statistical analyses

Progression free survival (PFS) was calculated in days from date of surgery until disease progression

or death from any cause. Kaplan-Meier curves were created to estimate and display the survival function for PFS. Dogs were censored if they were alive at the time of reporting or lost to follow-up prior to documentation of disease progression or death.

CD3, FoxP3, and GZB TIL densities were converted to binary variables according to whether a value was above or below the median value and were evaluated for association with PFS. Kaplan-Meier curves were compared using the log-rank test. Cox proportional-hazards regression models with single predictor variables were used to estimate hazard ratios, and the log-rank test was used to determine the significance of hazard ratios based on these models. The proportional hazards assumptions were met for all variables and validated based on scaled Schoenfeld residuals. Multiple variable models were not performed due to the population size of the study limiting the ability to interpret such data. Correlation analyses were performed using Spearman correlation. Statistical significance was established at $P < 0.05$. Statistical analyses were performed by a statistician (NK) using the survival package for R 4.3.2 (Eye Holes)(R Core Team, 2023).

## 3. Results

### 3.1. Patient characteristics

Sixteen dogs diagnosed with canine RCC that met the inclusion criteria were included. Represented

breeds included mixed breed (n = 6) and a single dog from the following pure breeds: Maltese, Labrador retriever, Pembroke Welsh terrier, bichon frisé, Portuguese water dog, Jack Russell terrier, English bulldog, golden retriever, American pit bull terrier, and cocker spaniel. The most common initial presenting complaints were a palpable abdominal mass (n=5) and lethargy (n=5), followed by hyporexia (n=4), hematuria (n=3), vomiting (n=2), and polyuria (n=1). All dogs were staged with thoracic and abdominal imaging at the time of diagnosis. Twelve dogs had thoracic radiographs and four dogs had thoracic computed tomography (CT). All dogs underwent abdominal ultrasound, with four also imaged with abdominal CT. No dogs had overt evidence of gross macroscopic metastasis at the time of ureteronephrectomy.

All sixteen dogs had a complete blood count (CBC) and chemistry panel performed prior to ureteronephrectomy. Three dogs were azotemic. Four dogs had elevated gamma-glutamyl transferase (GGT) without concurrent alanine transaminase (ALT) elevation, although one dog had concurrent alkaline phosphatase (ALP) elevation at 353 U/L. Nine dogs had a urinalysis performed at the time of diagnosis. Seven of nine dogs had gross and/or microscopic hematuria, four had epithelial cells detected, three had pyuria, two had glucosuria, and eight had proteinuria. The clinical characteristics and select baseline hematologic values for each patient at the time of diagnosis are summarized in Table 1 & 2.

### 3.2. Clinical course and treatment outcomes

All dogs underwent unilateral ureteronephrectomy. Fifteen dogs survived until discharge from the

hospital following surgery. One dog was euthanized in-hospital 48 hours after surgery due to septicemia and multiple organ dysfunction syndrome and was excluded from survival analysis. Three dogs received adjuvant chemotherapy at the discretion of the overseeing veterinarian, with doxorubicin (n=2) or toceranib phosphate

(n=1).

Four patients developed suspected tumor recurrence within the retroperitoneal space, confirmed

cytologically as carcinoma in one case. Six patients developed suspected metastatic disease in one or more anatomic sites, including pulmonary (n=5), locoregional lymph nodes (n=3), peritoneum (n=2), liver (n=1), subcutaneous (n=1), and retrobulbar space (n=1). Suspected metastatic lesions were not sampled, except the subcutaneous lesion which was confirmed cytologically as carcinoma. Death was

**Table 1**
Clinical characteristics of 16 canine patients with renal cell carcinoma at diagnosis.

| Variable | Number |
|---|---|
| Age (years), median (range) | 11 (4–13) |
| Weight (kilograms), median (range) | 12.4 (4.5–38) |
| Sex | |
| Male, castrated | 5 |
| Female, castrated | 11 |
| Location | |
| Left kidney | 9 |
| Right kidney | 7 |
| Tumor size (centimeters), median (range) | 7.1 (2.5–21) |
| Metastases (at diagnosis) | |
| None | 16 |
| Treatment | |
| Ureteronephrectomy | 16 |
| Adjuvant chemotherapy | 3 |

**Table 2**
Hematologic findings of 16 canine patients with renal cell carcinoma at diagnosis.

| Hematologic variable | Group | Number | Median (range) | Laboratory reference range |
|---|---|---|---|---|
| Hematocrit (%) | Above | 0 | - | 41–58% |
| | Within range | 11 | 47.3 (41.4–53) | |
| | Below | 5 | 36 (31.1–39.8) | |
| Neutrophil count ($10^3$/μL) | Above | 11 | 12.4 (9.6–17.5) | 2.7–9.4 |
| | Within range | 5 | 7.1 (5.0–9.2) | |
| | Below | 0 | - | |
| Lymphocyte count ($10^3$/μL) | Above | 0 | - | 0.9–4.7 |
| | Within range | 11 | 1.5 (1–2.11) | |
| | Below | 5 | 0.6 (0.2–0.8) | |
| Monocyte count ($10^3$/μL) | Above | 3 | 2.4 (1.4–2.8) | 0.1–1.3 |
| | Within range | 13 | 0.6 (0.1–1.3) | |
| | Below | 0 | - | |
| Platelet count ($10^3$/μL) | Above | 0 | - | 186–545 |
| | Within range | 15 | 397 (206–537) | |
| | Below | 1 | 163 | |
| BUN (mg/dL) | Above | 4 | 36 (31–64) | 5–30 |
| | Within range | 12 | 16.5 (10–30) | |
| | Below | 0 | - | |
| Creatinine (mg/dL) | Above | 3 | 2 (2–2.4) | 0.7–1.8 |
| | Within range | 12 | 1.0 (0.7–1.5) | |
| | Below | 1 | 0.6 | |
| Gamma-glutamyl transferase (U/L) | Above | 4 | 38 (31–73) | 7–24 |
| | Within range | 12 | 10.5 (3–19) | |
| | Below | 0 | - | |
| Alanine transaminase (U/L) | Above | 0 | - | 16–91 |
| | Within range | 15 | 42 (24–90) | |
| | Below | 1 | 16 | |
| Alkaline phosphatase (U/L) | Above | 4 | 347 (331–819) | 20–155 |
| | Within range | 11 | 106 (22–144) | |
| | Below | 1 | 17 | |

attributed to tumor-related causes in six patients that experienced progressive disease following discharge from surgery. Additional causes of death included: decreased mobility (n=1), acute decline in quality of life (n=1), oral malignant melanoma (n=1), or unknown (n=2). Only the patient that was euthanized due to decreased mobility underwent necropsy examination. No evidence of RCC recurrence was found, however, primary pulmonary carcinoma was incidentally detected.

For the fifteen dogs surviving until discharge, the median PFS was 524 days. Three patients were censored from PFS analysis: two were alive at the time of analysis (614 and 709 days post-nephrectomy) and one patient was lost to follow-up prior to documentation of disease progression or death at 51 days.

### 3.3. Histologic evaluation and CD3, FoxP3, and GZB quantification in canine RCC biopsies

The histologic features of all sixteen tumors are described in Table 3. Immunohistochemical staining for CD3, FoxP3 and GZB alongside TIL quantification algorithms of a representative RCC tumor with TIL densities approximating the median values for the cohort is shown in Fig. 1. The distribution for each stain, with median counts of 60, 11, and 10.5 cells/mm$^2$ for CD3, FoxP3, and GZB positivity were recorded (Fig. 1**C, F, I**). The highest CD3+ TIL count was 295 cells/mm$^2$ (range: 7–295 cells/mm$^2$). Moderate and statistically significant positive correlations were found between CD3 density and MC **(**Fig. 2**A)**, CD3 and FoxP3 densities **(**Fig. 2**B)**, and CD3 and GZB densities **(**Fig. 2**C)**. CD3, FoxP3 and GZB positive T cells were found scattered throughout all tumors with similar distributions, without obvious lymphoid aggregates near or within vascular spaces (Dieu-Nosjean et al., 2014).

### 3.4. Association of CD3, FoxP3, and GZB positive TIL density with patient outcome and distribution across different histopathologic subtypes

The raw cell counts for each marker and PFS for each patient is summarized in Table 4. Neither

CD3+ nor GZB+ TIL density was found to be associated with outcome (Fig. 3**A-B,** Table S1). Increased

**Table 3**
Histologic features of 16 canine renal cell carcinoma tumors.

| Histological feature | Groups | Number |
|---|---|---|
| Subtype | Papillary | 6 |
| | Tubular | 5 |
| | Solid | 4 |
| | Multilocular cystic | 1 |
| Clear cell morphology | Yes | 6 |
| | No | 10 |
| Mitotic count | < 10 | 4 |
| | 10–30 | 7 |
| | > 30 | 5 |
| Fuhrman nuclear grade | 2 | 4 |
| | 3 | 9 |
| | 4 | 3 |
| Vascular invasion | Yes | 1 |
| | No | 15 |
| Local invasiveness | Mild | 9 |
| | Moderate | 3 |
| | Severe | 4 |
| Sarcomatoid Change | Yes | 1 |
| | No | 15 |
| CD3/mm$^2$ | < 60 | 8 |
| | ≥ 60 | 8 |
| FoxP3/mm$^2$ | < 11 | 8 |
| | ≥ 11 | 8 |
| GZB/mm$^2$ | < 10.5 | 7 |
| | ≥ 10.5 | 9 |
| CD3: FoxP3 | < 5 | 8 |
| | ≥ 5 | 8 |
| GZB: FoxP3 | < 1 | 8 |
| | ≥ 1 | 8 |

FoxP3+ TIL density was negatively associated with PFS (p = 0.02, Fig. 3**C**). PFS for dogs with FoxP3+ TIL density above the median was shorter (273 days) compared to those with FoxP3+ TIL density below the median (1201 days). An increased ratio of GZB: FoxP3 TIL density was positively associated with PFS (p =

0.006, Fig. 3**D**).

Due to the association between FoxP3+ cell density and PFS, the density distribution of each T cell marker across different histopathologic subgroupings was investigated. CD3, FoxP3, and GZB positive cell density appeared similar across papillary, tubular, and multilocular cystic subtypes (Fig. 4). The highest FoxP3+ densities were found in tumors of the solid subtype; however, statistical comparisons were not performed due to low case numbers of each subtype.

## 4. Discussion

Although human RCC is considered highly immunogenic with most tumors being heavily infiltrated with TIL, the overall TIL density of canine RCC tumors in our study was low (Nakano et al., 2001; Steindl et al., 2021). Nearly an 8-fold higher median density of 454 CD3+ TIL/mm$^2$ in human RCC tumors has been reported, compared to a median density of 60 CD3+ TIL/mm$^2$ in our canine RCC samples (Steindl et al., 2021). Similarly, canine RCC TIL density is sparse in comparison to other canine tumor types, such as localized histiocytic sarcoma (Lenz et al., 2022). The highest CD3+ TIL count observed in our set of canine RCC tumors was 295 cells/mm$^2$, whereas 67% of canine localized histiocytic sarcoma tumor samples had

CD3+ TIL densities >1000 cells/mm$^2$ (Lenz et al., 2022). Potential underlying reasons for lack of CD3, FoxP3, and GZB positive T cell infiltration in canine RCC are currently unknown. Neoantigens arising from somatic mutations can engage endogenous anti-tumor T cells, thus it is possible that canine RCC has fewer somatic mutations, resulting in lower CD3, FoxP3, and GZB TIL densities (Brochier et al., 2023). Mitotic count was positively associated with CD3 TIL density in our canine cohort, suggesting that more mitotically active tumors may be more immunogenic. However, the tumor microenvironment of canine RCC is likely to have additional mechanisms driving TIL exclusion and immune evasion, including soluble, cellular, and stromal components (Joyce and Fearon, 2015). Further investigation as to why canine RCC is immunologically quiescent is needed, which in turn may inform potential therapeutic strategies to enable optimal immune targeting of canine RCC.

The low CD3, FoxP3, and GZB TIL densities found in our study suggest checkpoint blockade may

have reduced efficacy in the treatment of dogs with RCC. However, it is important to note that while this is the first description of T cell subsets in canine RCC, it is not a comprehensive characterization of immunologic landscape nor T cell function (Hay and Slansky, 2022). Although GZB is often used to gauge T cell activation, demonstration of GZB protein expression alone is not sufficient to predict T cell function and GZB may also be expressed by other lymphoid subsets including natural killer (NK) cells (Hay and Slansky, 2022). Costaining with additional markers, such as perforin, was not performed, and would have supplemented our functional assessment of GZB+ TIL. Additionally, other cellular or humoral factors that contribute to tumor immunogenicity have not been fully characterized in this work, and the interactions between canine RCC and the immune system is not well-documented. Future studies are needed to more fully characterize the immune genetic signature of canine RCC.

Notably, despite an overall low TIL density, increased FoxP3+ TIL density was negatively associated

with patient outcome in our cohort of dogs with RCC. This is in alignment with clinical findings in human RCC, as multiple studies have found increased density of intratumoral Tregs is associated with worse patient outcome (Bai et al., 2021; Jensen et al., 2009; Liotta et al., 2011; Senbabaoglu et al., 2016). Regulatory T cells are prominent cellular mediators capable of suppressing anti-tumor immune responses,

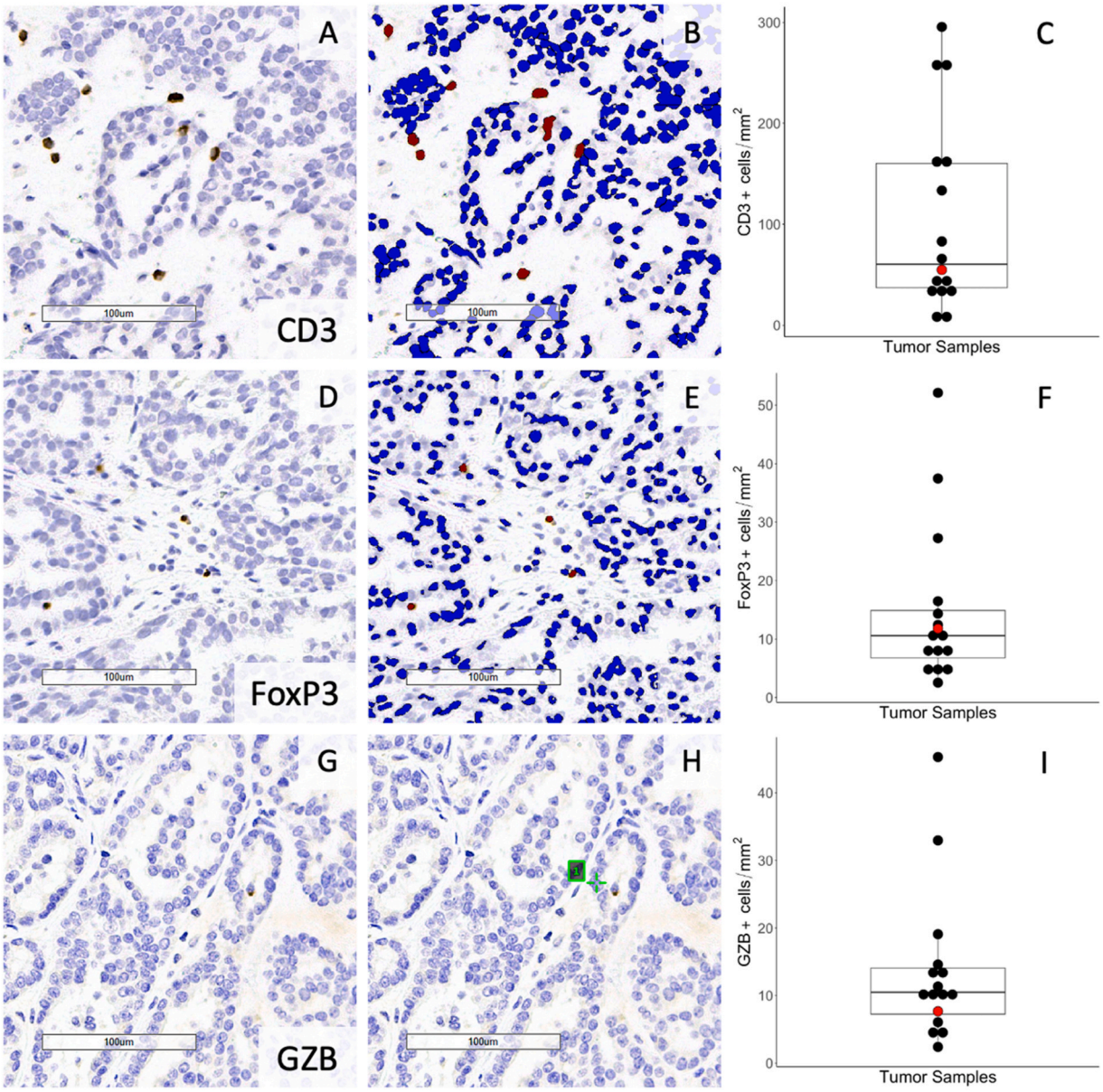


**Fig. 1.** CD3, FoxP3, and granzyme B immunostaining of a renal carcinoma from an 11-year-old female spayed mixed breed dog with TIL densities approximating the median value for the cohort. **(A)** IHC staining for CD3, **(B)** application of nuclear quantification algorithm, and **(C)** distribution of CD3 quantification across all tumor samples. **(D)** IHC staining for FoxP3, **(E)** application of nuclear quantification algorithm, and **(F)** distribution of FoxP3 quantification across all tumor samples. **(G)** IHC staining for granzyme B (GZB), **(H)** manual quantification of digitally captured image, and **(I)** distribution of GZB quantification across all tumor samples. IHC staining detected using DAB and counterstained with hematoxylin, scale bars—100 μm, negatively stained cells are labeled blue and positively stained cells labeled red in the applied algorithms **(B&E)**, manually counted cells are labeled on digitally captured slides by enumeration in green font **(H)**. CD3, FoxP3, and GZB-positive TIL densities for the pictured case are identified in red with the horizontal bar marking median value for the cohort **(C, F, I)**. Immunohistochemical, IHC; granzyme B, GZB; diaminobenzidine chromogen, DAB.

promoting tumor progression (Joyce and Fearon, 2015). While our data provide exciting preliminary evidence, the prognostic significance of FoxP3 positive TIL density in canine RCC requires additional investigation in a larger patient cohort.

To investigate the potential influence of histopathologic subtype on T cell infiltration, CD3, FoxP3, and GZB density was compared between groups. The solid subtype appeared to have greater FoxP3 TIL infiltration compared with other subtypes, despite similar GZB density. Interestingly, these patients also experienced short survival times with a median PFS of 64 days. Histopathologic subtyping of canine RCC is less characterized than in human medicine. The most recent classification in human RCC contains 16 distinct types based on molecular and immunophenotypic features, carrying varied prognoses and response to immune checkpoint blockade (Young et al., 2018; Zhang et al., 2021). Multilocular cystic is a rare form of RCC in humans that carries a good prognosis with low metastatic potential (Suzigan et al., 2006). Canine multilocular cystic tumors appear to carry a similar favorable outcome and metastasis has not been reported for this histologic subtype (Edmondson et al., 2015). The single case in our study also experienced prolonged survival and was alive at the time of writing with no detection of metastatic disease at 614 days. Future studies to molecularly characterize and more comprehensively assess the immunologic landscape of canine RCC subtypes may aid in our understanding of immune cell infiltration patterns, clinical behavior, and response to immune checkpoint inhibitors.

Our study had several limitations. Due to the rare nature of RCC in

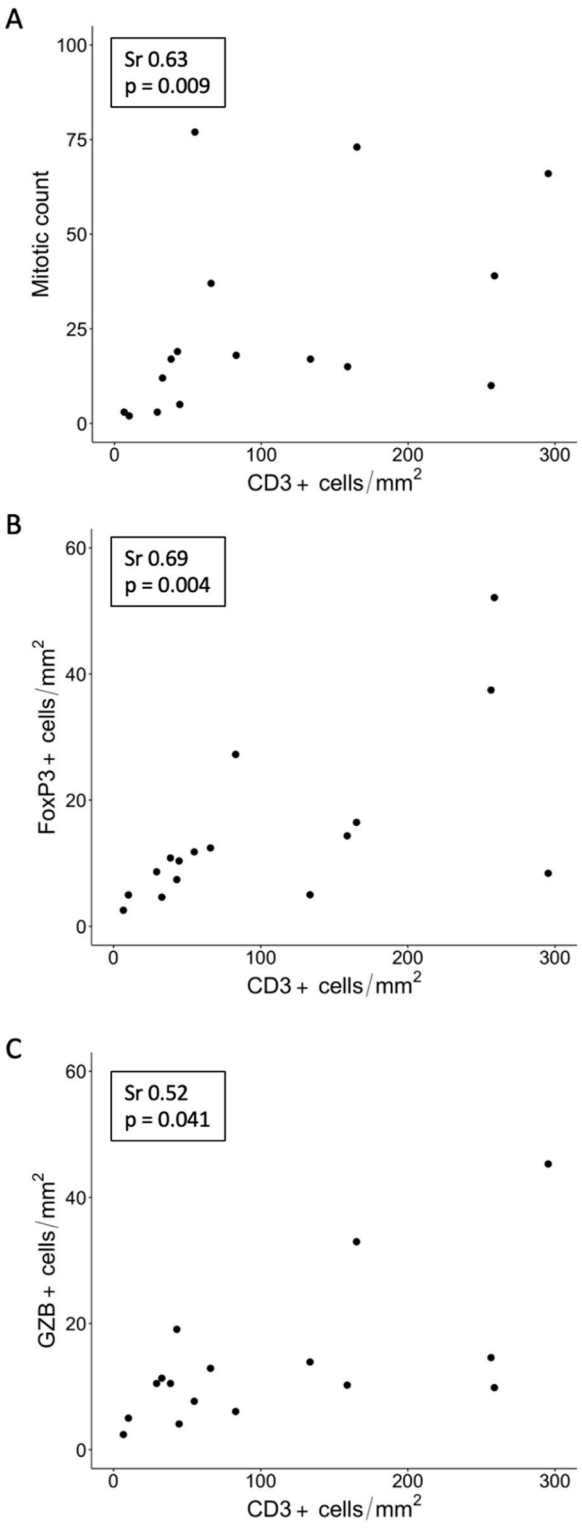


**Fig. 2.** Scatter plots for 16 dogs with renal carcinoma treated with nephrectomy revealing correlations between **(A)** CD3 TIL density and mitotic count (MC), **(B)** CD3 and FoxP3 TIL density, and **(C)** CD3 and granzyme B (GZB) TIL density. Spearman's rho (Sr) and p values displayed for each plot.

dogs, our study evaluated a small

population of patients despite a database search over thirteen years. While all patients were fully staged and treated with ureteronephrectomy, case management varied regarding use of adjuvant chemotherapy and monitoring schedule. Further, as a retrospective

**Table 4**
CD3, FoxP3, and granzyme B (GZB) positive cell density and progression free survival (PFS) of 15 dogs with renal carcinoma treated with ureteronephrectomy that survived until discharge. Censored events are listed in parentheses.

| Patient | CD3 cells/ mm$^2$ | FoxP3 cells/ mm$^2$ | GZB cells/ mm$^2$ | GZB: FoxP3 Ratio | PFS |
|---|---|---|---|---|---|
| 1 | 257 | 37 | 15 | 0.4 | 14 |
| 2 | 83 | 27 | 6 | 0.2 | 40 |
| 3 | 159 | 14 | 10 | 0.7 | 88 |
| 4 | 295 | 8 | 45 | 5.4 | 189 |
| 5 | 39 | 11 | 11 | 1.0 | 249 |
| 6 | 55 | 12 | 8 | 0.7 | 297 |
| 7 | 165 | 16 | 33 | 2.0 | 459 |
| 8 | 43 | 7 | 19 | 2.6 | 524 |
| 9 | 259 | 52 | 10 | 0.2 | 566 |
| 10 | 29 | 9 | 11 | 1.2 | (614) |
| 11 | 133 | 5 | 14 | 2.8 | (709) |
| 12 | 66 | 12 | 13 | 1.0 | 1096 |
| 13 | 10 | 5 | 5 | 1.0 | 1201 |
| 14 | 33 | 5 | 11 | 2.5 | 1322 |
| 15 | 7 | 3 | 2 | 0.9 | (51) |

analysis, there is the potential to introduce bias from a nonrandomly sampled patient population. Additionally, reagents available to interrogate the tumor immune microenvironment at the protein level in canine tumors are currently limited, including no well-described antiCD8 antibody that binds to canine CD8 in FFPE tissues. Granzyme B was used as a surrogate for cytotoxic T cells; however, this marker lacks specificity for cytotoxic T cells as GZB can also be expressed in the granules of natural killer (NK) cells. However, prior work in canine histiocytic sarcoma revealed cellular co-expression of CD3 and GZB, consistent with the majority of GZB+ cells being of T cell and not NK cell lineage (Lenz et al., 2022). Similarly, while FoxP3 expression is a useful marker for identification and quantification of Tregs in dogs, there is the possibility that quantification of FoxP3 immunostaining captured cells other than Tregs. FoxP3 expression has been reported in other human and murine lymphoid, myeloid, and epithelial cells (Biller et al., 2007; Devaud et al., 2014). However, FoxP3 expression in cells other than Tregs in dogs is not welldocumented. Further, IHC staining for CD31 was not performed, which would have aided our interpretation for the spatial distribution of TIL subsets assessed. While our panel is limited, the widely applied

Immunoscore used to appraise the immune contexture of multiple human tumors is similarly based solely on CD3 and CD8 infiltrates, yet remains a powerful tool with which to study the immune tumor microenvironment (Angell et al., 2020).

In general, there is lack of standardization of TIL assessment across different studies published to date (Inoue et al., 2017; Lenz et al., 2022; Pinard et al., 2022). The algorithms for CD3 and FoxP3 cell counting utilized in the current study are publicly available through ImageScope software, however, a consensus is needed to standardize the appraisal of TIL in a research setting, as well as standard histopathologic practice and clinical trials (Salgado et al., 2015). While automated cell counts improve accuracy, the staining pattern of granular uptake limited our ability to build an algorithm for quantification of GZB immunoreactivity. As manual counts are less precise compared with machine-based quantification, the data for GZB must be considered a semi-quantitative approximation. A standardized methodology for quantifying and reporting TIL, as well as determining meaningful cut-off values for survival analyses, is needed to improve study comparison and to evaluate the prognostic significance of TIL for canine cancer patients.

## 5. Conclusion

In conclusion, CD3, FoxP3, and GZB TIL densities in canine RCC are low in comparison to human

RCC and other tumor types in veterinary medicine. Comprehensive

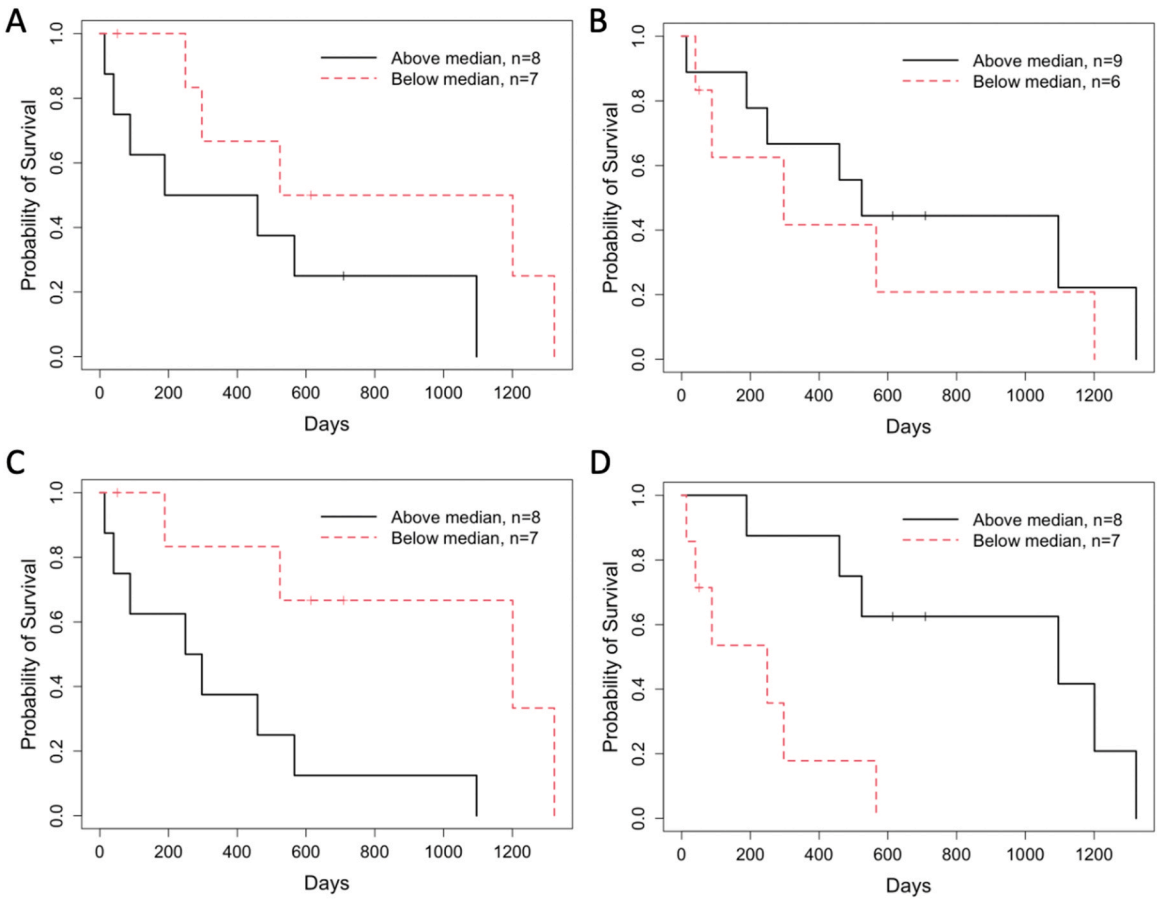


**Fig. 3.** Kaplan-Meier curves depicting progression free survival (PFS) for 15 dogs with renal carcinoma treated with ureteronephrectomy that survived until discharge stratified by T cell infiltration (TIL) densities of (**A)** CD3 positive TIL counts, (**B)** granzyme B (GZB) positive TIL counts, (**C)** FoxP3 positive TIL counts, and (**D)** ratio of GZB: FoxP3 positive TIL counts. Cases were classified as having a high or low TIL density according to the median density of all cases. Hash marks indicate censored events.

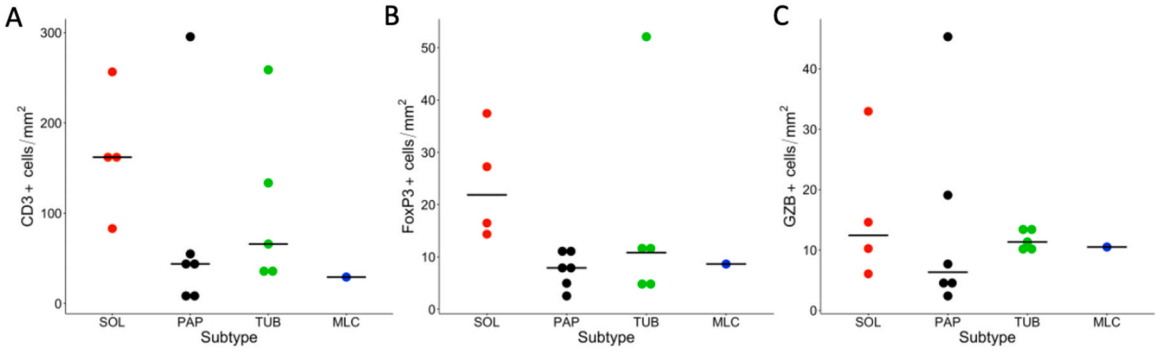


**Fig. 4.** Dot plot showing distribution of CD3, FoxP3, and granzyme B (GZB) positive TIL counts for each histopathologic subtype. Horizontal bars indicate median value. Median CD3+ densities for solid, papillary, tubular, and MLC tumors were 162, 43.7, 65.8, and 29.2 cells/mm$^2$ respectively. Median FoxP3+ densities for solid, papillary, tubular, and MLC tumors were 21.9, 7.9, 10.8, and 8.6 cells/mm$^2$. Median GZB+ densities for solid, papillary, tubular, and MLC tumors were 12.4, 6.3, 11.3, and 10.5 cells/mm$^2$. Solid, SOL; Papillary, PAP; Tubular, TUB; Multilocular cystic, MLC.

characterization of the TME in canine RCC is needed to guide therapeutic approaches and development. Increased FoxP3+ TIL density was associated with worse patient outcome in our small cohort of dogs, and the potential prognostic significance of FoxP3+ TIL density in canine RCC warrants additional study in a larger cohort of patients.

## Funding

This work was supported by the Miso Harris Fund donated to the Comprehensive Cancer Care service; internal funds provided to Jennifer A Lenz by the University of Pennsylvania School of Veterinary Medicine; Abramson Cancer Center (P30 CA016520); and the National Institutes of Health Shared Instrumentation Grant (S10 OD023465–01A1). Matthew J Atherton is supported by NIH/NCI K08CA252619.

## CRediT authorship contribution statement

**Jennifer A Lenz:** Conceptualization, Data curation, Formal analysis,

Funding acquisition, Investigation, Methodology, Project administration, Resources, Supervision, Visualization, Writing – original draft, Writing – review & editing. **Matthew J Atherton:** Conceptualization, Formal analysis, Funding acquisition, Supervision, Writing – original draft, Writing – review & editing. **Ashleigh Cournoyer:** Data curation, Investigation, Methodology, Writing – original draft, Writing – review & editing. **Charles-Antoine Assenmacher:** Data curation, Formal analysis, Investigation, Methodology, Software, Supervision, Validation, Visualization, Writing – review & editing, Funding acquisition. **Hayley Amerman:** Data curation, Investigation, Methodology, Visualization, Writing – review & editing. **James A Perry:** Conceptualization, Supervision, Writing – review & editing. **Amy Durham:** Data curation, Investigation, Supervision, Writing – review & editing. **Nicholas Keuler:** Formal analysis, Methodology, Writing – review & editing. **Allison Gedney:** Data curation, Writing – review & editing.

## Declaration of Competing Interest

The authors declare the following financial interests/personal relationships which may be considered as potential competing interests: Matthew Atherton reports financial support was provided by National Institutes of Health, NCI, K08CA252619. Charles-Antoine Assenmacher reports financial support was provided by National Institutes of Health Shared Instrumentation Grant (S10 OD023465–01A1). Charles-Antoine Assenmacher reports financial support was provided by Abramson Cancer Center (P30 CA016520). Jennifer Lenz reports financial support was provided by Miso Harris Fund donated to Penn Vet Comprehensive Cancer Care service. If there are other authors, they declare that they have no known competing financial interests or personal relationships that could have appeared to influence the work reported in this paper.

## Acknowledgements

The authors would like to thank Enrico Radaelli and the Comparative Pathology Core for immunohistochemical validation and contribution to study design.

## Appendix A. Supporting information

Supplementary data associated with this article can be found in the online version at doi:10.1016/j.vetimm.2024.110741.

## References

Angell, H.K., Bruni, D., Barrett, J.C., Herbst, R., Galon, J., 2020. The immunoscore: colon cancer and beyond. Clin. Cancer Res. 26, 332–339.
Bai, D., Feng, H., Yang, J., Yin, A., Qian, A., Sugiyama, H., 2021. Landscape of immune cell infiltration in clear cell renal cell carcinoma to aid immunotherapy. Cancer Sci. 112, 2126–2139.
Biller, B.J., Elmslie, R.E., Burnett, R.C., Avery, A.C., Dow, S.W., 2007. Use of FoxP3 expression to identify regulatory T cells in healthy dogs and dogs with cancer. Vet. Immunol. Immunopathol. 116, 69–78.
Brochier, W., Bricard, O., Coulie, P.G., 2023. Facts and hopes in cancer antigens recognized by T cells. Clin. Cancer Res. 29, 309–315.
Bryan, J.N., Henry, C.J., Turnquist, S.E., Tyler, J.W., Liptak, J.M., Rizzo, S.A., Sfiligoi, G., Steinberg, S.J., Smith, A.N., Jackson, T., 2006. Primary renal neoplasia of dogs. J. Vet. Intern. Med. 20, 1155–1160.
Devaud, C., Darcy, P.K., Kershaw, M.H., 2014. Foxp3 expression in T regulatory cells and other cell lineages. Cancer Immunol. Immunother. 63, 869–876.
Diaz-Montero, C.M., Rini, B.I., Finke, J.H., 2020. The immunology of renal cell carcinoma. Nat. Rev. Nephrol. 16, 721–735.
Dieu-Nosjean, M.C., Goc, J., Giraldo, N.A., Sautes-Fridman, C., Fridman, W.H., 2014. Tertiary lymphoid structures in cancer and beyond. Trends Immunol. 35, 571–580.
Edmondson, E.F., Hess, A.M., Powers, B.E., 2015. Prognostic significance of histologic features in canine renal cell carcinomas: 70 nephrectomies. Vet. Pathol. 52, 260–268.
Fuhrman, S.A., Lasky, L.C., Limas, C., 1982. Prognostic significance of morphologic parameters in renal cell carcinoma. Am. J. Surg. Pathol. 6, 655–663.
Galon, J., Bruni, D., 2019. Approaches to treat immune hot, altered and cold tumours with combination immunotherapies. Nat. Rev. Drug Discov. 18, 197–218.
Galon, J., Costes, A., Sanchez-Cabo, F., Kirilovsky, A., Mlecnik, B., Lagorce-Pages, C., Tosolini, M., Camus, M., Berger, A., Wind, P., Zinzindohoue, F., Bruneval, P., Cugnenc, P.H., Trajanoski, Z., Fridman, W.H., Pages, F., 2006. Type, density, and location of immune cells within human colorectal tumors predict clinical outcome. Science 313, 1960–1964.
Griffiths, R.W., Elkord, E., Gilham, D.E., Ramani, V., Clarke, N., Stern, P.L., Hawkins, R. E., 2007. Frequency of regulatory T cells in renal cell carcinoma patients and investigation of correlation with survival. Cancer Immunol. Immunother. 56, 1743–1753.
Gulati, S., Vaishampayan, U., 2020. Current state of systemic therapies for advanced renal cell carcinoma. Curr. Oncol. Rep. 22, 26.
Hay, Z.L.Z., Slansky, J.E., 2022. Granzymes: the molecular executors of immune-mediated cytotoxicity. Int. J. Mol. Sci. 23.
Inoue, A., Maeda, S., Kinoshita, R., Tsuboi, M., Yonezawa, T., Matsuki, N., 2017. Density of tumorinfiltrating granzyme B-positive cells predicts favorable prognosis in dogs with transitional cell carcinoma. Vet. Immunol. Immunopathol. 190, 53–56.
Jensen, H.K., Donskov, F., Nordsmark, M., Marcussen, N., von der Maase, H., 2009. Increased intratumoral FOXP3-positive regulatory immune cells during interleukin-2 treatment in metastatic renal cell carcinoma. Clin. Cancer Res. 15, 1052–1058.
Joyce, J.A., Fearon, D.T., 2015. T cell exclusion, immune privilege, and the tumor microenvironment. Science 348, 74–80.
Kim, J.H., Chon, S.K., Im, K.S., Kim, N.H., Sur, J.H., 2013. Correlation of tumor-infiltrating lymphocytes to histopathological features and molecular phenotypes in canine mammary carcinoma: a morphologic and immunohistochemical morphometric study. Can. J. Vet. Res. 77, 142–149.
Klein, M.K.C., G.C, Harris, C.K., 1987. Canine primary renal neoplasms: a retrospective review of 54 cases. J. Am. Anim. Hosp. Assoc. 24, 443–452.
Kumar, A., Watkins, R., Vilgelm, A.E., 2021. Cell therapy with TILs: training and taming T cells to fight cancer. Front. Immunol. 12, 690499.
Lenz, J.A., Assenmacher, C.A., Costa, V., Louka, K., Rau, S., Keuler, N.S., Zhang, P.J., Maki, R.G., Durham, A.C., Radaelli, E., Atherton, M.J., 2022. Increased tumor-infiltrating lymphocyte density is associated with favorable outcomes in a comparative study of canine histiocytic sarcoma. Cancer Immunol. Immunother. 71, 807–818.
Liotta, F., Gacci, M., Frosali, F., Querci, V., Vittori, G., Lapini, A., Santarlasci, V., Serni, S., Cosmi, L., Maggi, L., Angeli, R., Mazzinghi, B., Romagnani, P., Maggi, E., Carini, M., Romagnani, S., Annunziato, F., 2011. Frequency of regulatory T cells in peripheral blood and in tumour-infiltrating lymphocytes correlates with poor prognosis in renal cell carcinoma. BJU Int. 107, 1500–1506.
Maeda, S., Motegi, T., Iio, A., Kaji, K., Goto-Koshino, Y., Eto, S., Ikeda, N., Nakagawa, T., Nishimura, R., Yonezawa, T., Momoi, Y., 2022. Anti-CCR4 treatment depletes regulatory T cells and leads to clinical activity in a canine model of advanced prostate cancer. J. Immunother. Cancer 10.
Maibach, F., Sadozai, H., Seyed Jafari, S.M., Hunger, R.E., Schenk, M., 2020. Tumor-infiltrating lymphocytes and their prognostic value in cutaneous melanoma. Front. Immunol. 11, 2105.
Motzer, R.J., Escudier, B., George, S., Hammers, H.J., Srinivas, S., Tykodi, S.S., Sosman, J.A., Plimack, E.R., Procopio, G., McDermott, D.F., Castellano, D., Choueiri, T.K., Donskov, F., Gurney, H., Oudard, S., Richardet, M., Peltola, K., Alva, A.S., Carducci, M., Wagstaff, J., Chevreau, C., Fukasawa, S., Tomita, Y., Gauler, T.C., Kollmannsberger, C.K., Schutz, F.A., Larkin, J., Cella, D., McHenry, M. B., Saggi, S.S., Tannir, N.M., 2020. Nivolumab versus everolimus in patients with advanced renal cell carcinoma: updated results with long-term follow-up of the randomized, open-label, phase 3 CheckMate 025 trial. Cancer 126, 4156–4167.
Nakano, O., Sato, M., Naito, Y., Suzuki, K., Orikasa, S., Aizawa, M., Suzuki, Y., Shintaku, I., Nagura, H., Ohtani, H., 2001. Proliferative activity of intratumoral CD8(+) T-lymphocytes as a prognostic factor in human renal cell carcinoma: clinicopathologic demonstration of antitumor immunity. Cancer Res. 61, 5132–5136.
Pinard, C.J., , International Immuno-Oncology Biomarker Working, Lagree, G., Lu, A., Klein, F.I., Oblak, J., Salgado, M.L., Cardenas, R., Brunetti, J.C.P., Muscatello, B., Sarli, L.V., Foschini, G., Hardas, M.P., Castillo, A., AbdulJabbar, S.P., Yuan, K., Moore, Y., Tran, D.A., W.T, 2022. Comparative evaluation of tumor-infiltrating lymphocytes in companion animals: immuno-oncology as a relevant translational model for cancer therapy. Cancers (Basel) 14.
Powles, T., Tomczak, P., Park, S.H., Venugopal, B., Ferguson, T., Symeonides, S.N., Hajek, J., Gurney, H., Chang, Y.H., Lee, J.L., Sarwar, N., Thiery-Vuillemin, A., Gross-Goupil, M., Mahave, M., Haas, N.B., Sawrycki, P., Burgents, J.E., Xu, L., Imai, K., Quinn, D.I., Choueiri, T.K., Investigators, K.-, 2022. Pembrolizumab versus placebo as post-nephrectomy adjuvant therapy for clear cell renal cell carcinoma (KEYNOTE-564): 30-month follow-up analysis of a multicentre, randomised, doubleblind, placebo-controlled, phase 3 trial. Lancet Oncol. 23, 1133–1144.
R. Core Team, 2023. R: A Language and Environment for Statistical Computing R Foundation for Statistical Computing, Vienna, Austria. <https://www.R-project.org/>.
Saleh, R., Elkord, E., 2020. FoxP3(+) T regulatory cells in cancer: Prognostic biomarkers and therapeutic targets. Cancer Lett. 490, 174–185.
Salgado, R., Denkert, C., Demaria, S., Sirtaine, N., Klauschen, F., Pruneri, G., Wienert, S., Van den Eynden, G., Baehner, F.L., Penault-Llorca, F., Perez, E.A., Thompson, E.A., Symmans, W.F., Richardson, A.L., Brock, J., Criscitiello, C., Bailey, H., Ignatiadis, M., Floris, G., Sparano, J., Kos, Z., Nielsen, T., Rimm, D.L., Allison, K.H., Reis-Filho, J.S., Loibl, S., Sotiriou, C., Viale, G., Badve, S., Adams, S., Willard-Gallo, K., Loi, S., International, T.W.G., 2015. The evaluation of tumor-infiltrating lymphocytes (TILs) in breast cancer: recommendations by an International TILs Working Group 2014. Ann. Oncol. 26, 259–271.
Sanchez-Gastaldo, A., Kempf, E., Gonzalez Del Alba, A., Duran, I., 2017. Systemic treatment of renal cell cancer: a comprehensive review. Cancer Treat. Rev. 60, 77–89.

Senbabaoglu, Y., Gejman, R.S., Winer, A.G., Liu, M., Van Allen, E.M., de Velasco, G., Miao, D., Ostrovnaya, I., Drill, E., Luna, A., Weinhold, N., Lee, W., Manley, B.J., Khalil, D.N., Kaffenberger, S.D., Chen, Y., Danilova, L., Voss, M.H., Coleman, J.A., Russo, P., Reuter, V.E., Chan, T.A., Cheng, E.H., Scheinberg, D.A., Li, M.O., Choueiri, T.K., Hsieh, J.J., Sander, C., Hakimi, A.A., 2016. Tumor immune microenvironment characterization in clear cell renal cell carcinoma identifies prognostic and immunotherapeutically relevant messenger RNA signatures. Genome Biol. 17, 231.

Steindl, A., Alpar, D., Heller, G., Mair, M.J., Gatterbauer, B., Dieckmann, K., Widhalm, G., Hainfellner, J.A., Schmidinger, M., Bock, C., Mullauer, L., Preusser, M., Berghoff, A.S., 2021. Tumor mutational burden and immune infiltrates in renal cell carcinoma and matched brain metastases. ESMO Open 6, 100057.

Suzigan, S., Lopez-Beltran, A., Montironi, R., Drut, R., Romero, A., Hayashi, T., Gentili, A.L., Fonseca, P.S., deTorres, I., Billis, A., Japp, L.C., Bollito, E., Algaba, F., Requena-Tapias, M.J., 2006. Multilocular cystic renal cell carcinoma: a report of 45 cases of a kidney tumor of low malignant potential. Am. J. Clin. Pathol. 125, 217–222.

Yasumaru, C.C., Xavier, J.G., Strefezzi, R.F., Salles-Gomes, C.O.M., 2021. Intratumoral T-lymphocyte subsets in canine oral melanoma and their association with clinical and histopathological parameters. Vet. Pathol. 58, 491–502.

Young, M.D., Mitchell, T.J., Vieira Braga, F.A., Tran, M.G.B., Stewart, B.J., Ferdinand, J. R., Collord, G., Botting, R.A., Popescu, D.M., Loudon, K.W., Vento-Tormo, R., Stephenson, E., Cagan, A., Farndon, S.J., Del Castillo Velasco-Herrera, M., Guzzo, C., Richoz, N., Mamanova, L., Aho, T., Armitage, J.N., Riddick, A.C.P., Mushtaq, I., Farrell, S., Rampling, D., Nicholson, J., Filby, A., Burge, J., Lisgo, S., Maxwell, P.H., Lindsay, S., Warren, A.Y., Stewart, G.D., Sebire, N., Coleman, N., Haniffa, M., Teichmann, S.A., Clatworthy, M., Behjati, S., 2018. Single-cell transcriptomes from human kidneys reveal the cellular identity of renal tumors. Science 361, 594–599.

Zhang, Y., Narayanan, S.P., Mannan, R., Raskind, G., Wang, X., Vats, P., Su, F., Hosseini, N., Cao, X., Kumar-Sinha, C., Ellison, S.J., Giordano, T.J., Morgan, T.M., Pitchiaya, S., Alva, A., Mehra, R., Cieslik, M., Dhanasekaran, S.M., Chinnaiyan, A.M., 2021. Single-cell analyses of renal cell cancers reveal insights into tumor microenvironment, cell of origin, and therapy response. Proc. Natl. Acad. Sci. U. S. A. 118.